ELASTIC STRESS ANALYSIS OF ADVANCED FUNCTIONALLY GRADED PLATES IMPACTED BY BLAST LOADING

Terry Hause, Ph.D.[a]

[a]Research Mechanical Engineer, U.S. Army RDECOM-TARDEC, Warren, MI 48397

ABSTRACT

The foundation of the theory of functionally graded plates with all four edges simply supported, under a Friedlander explosive spherical air-blast, is developed, within the classical plate theory (CPT). The constituent materials, ceramic and metal, vary across the wall thickness according to a prescribed power law. The theory incorporates the geometrical nonlinearities, the dynamic effects, compressive/tensile edge loadings, damping effects, and the structural symmetries (symmetric and asymmetric). The static and dynamic solutions are developed leveraging the use of a stress potential coupled with the Extended-Galerkin method and the Runge-Kutta method. Validations with simpler cases existing within the literature are made. The analysis focuses on how to alleviate the unwanted effects of large elastic stresses and deformations through material selection and proper gradation of the constitutive phases.

Key Words: Functionally Graded; Explosive Blast, Dynamic Response, Elastic Stress

1. INTRODUCTION

During military conflicts, the structure of army military vehicles may have to withstand blast loading, the residual effects of which are the blast pressure, fragmentation, and heat. Advances in functionally graded materials, which combine the properties of two dissimilar materials, has been a motivating factor in viewing these types of materials has a viable alternative to the current metallic structures being utilized. Functionally graded materials (FGM's) are high-performance heat resistant materials able to withstand ultrahigh temperatures and extremely large thermal

Report Documentation Page

Form Approved
OMB No. 0704-0188

1. REPORT DATE	2. REPORT TYPE	3. DATES COVERED
18 JAN 2010	**Technical Report**	**18-01-2010 to 18-01-2010**

4. TITLE AND SUBTITLE
ELASTIC STRESS ANALYSIS OF ADVANCED FUNCTIONALLY GRADED PLATES IMPACTED BY BLAST LOADING

5a. CONTRACT NUMBER

5b. GRANT NUMBER

5c. PROGRAM ELEMENT NUMBER

6. AUTHOR(S)
Terry Hause

5d. PROJECT NUMBER

5e. TASK NUMBER

5f. WORK UNIT NUMBER

7. PERFORMING ORGANIZATION NAME(S) AND ADDRESS(ES)
U.S. Army TARDEC ,6501 E.11 Mile Rd,Warren,MI,48397-5000

8. PERFORMING ORGANIZATION REPORT NUMBER
#21440

9. SPONSORING/MONITORING AGENCY NAME(S) AND ADDRESS(ES)
U.S. Army TARDEC, 6501 E.11 Mile Rd, Warren, MI, 48397-5000

10. SPONSOR/MONITOR'S ACRONYM(S)
TARDEC

11. SPONSOR/MONITOR'S REPORT NUMBER(S)
#21440

12. DISTRIBUTION/AVAILABILITY STATEMENT
Approved for public release; distribution unlimited

13. SUPPLEMENTARY NOTES
Submitted to International Journal of Solids and Structures.

14. ABSTRACT
The foundation of the theory of functionally graded plates with all four edges simply supported, under a Friedlander explosive spherical air-blast, is developed, within the classical plate theory (CPT). The constituent materials, ceramic and metal, vary across the wall thickness according to a prescribed power law. The theory incorporates the geometrical nonlinearities, the dynamic effects, compressive/tensile edge loadings, damping effects, and the structural symmetries (symmetric and asymmetric). The static and dynamic solutions are developed leveraging the use of a stress potential coupled with the Extended-Galerkin method and the Runge-Kutta method. Validations with simpler cases existing within the literature are made. The analysis focuses on how to alleviate the unwanted effects of large elastic stresses and deformations through material selection and proper gradation of the constitutive phases.

15. SUBJECT TERMS
Functionally Graded; Explosive Blast, Dynamic Response, Elastic Stress

16. SECURITY CLASSIFICATION OF:			17. LIMITATION OF ABSTRACT	18. NUMBER OF PAGES	19a. NAME OF RESPONSIBLE PERSON
a. REPORT	b. ABSTRACT	c. THIS PAGE			
unclassified	**unclassified**	**unclassified**	**Same as Report (SAR)**	**37**	

Standard Form 298 (Rev. 8-98)
Prescribed by ANSI Std Z39-18

gradients. The FGM's are microscopically inhomogeneous with thermo-mechanical properties which vary smoothly and continuously from one surface to another. These graded structures allow the integration of dissimilar materials, like ceramics and metals that combine different or even incompatible properties such as hardness and toughness. In addition, by varying both the material selection and the prescribed variation of the two constituent materials from one surface to another, it is believed that the excessive stresses and deflections can be diminished resulting in many benefits to the survivability of the soldier.

These facts necessitates the need to gain an understanding of the response behavior and the load carrying capacity of plate-type structures composed of both symmetric and asymmetric-type symmetries of functionally graded plate-type structures exposed to blast loading and to gain an understanding of how varying both the material selection and the prescribed variation of the two constituent materials from one surface to another can alleviate the excessive mechanical stresses and deflections occurring during a blast event.

2. BASIC ASSUMPTIONS AND PRELIMINARIES

The plate mid surface is referred to a cartesian orthogonal system of coordinates (x,y,z), while z is the thickness coordinate measured positive in the upwards direction from the mid-surface of the plate with h being the uniform plate thickness of the plate, and y is directed perpendicular to the x-axis in the plane of the plate. See Fig. 1 below.

The nonlinear elastic theory of FG Plates is developed using the classical plate deformation Theory [6]. It is also assumed that the FG plate is made-up of ceramic and metal phases whose material properties vary smoothly and continuously across the wall thickness. By applying the rule of mixtures, the material properties such as Young's Modulus, Density, and Poisson's Ratio are assumed to vary across the wall thickness as

$$P(z) = P_c V_c(z) + P_m V_m(z)\,, \tag{1}$$

in which P_c and P_m denote the material properties of the ceramic and metallic phases, of the plate, respectively. $V_c(z)$ and $V_m(z)$ are correspondingly, the volume fractions of the ceramic and metal respectively, fulfilling the relation

$$V_c(z) + V_m(z) = 1\,. \tag{2}$$

By virtue of (2), Eq. (1) can be expressed as

$$P(z) = (P_c - P_m)V_c(z) + P_m\,. \tag{3}$$

By observation, one can deduce that for $V_c(z) = 0$, $P(z) = P_m$ and for $V_c = 1$, $P(z) = P_c$. As a result, $V_c(z) \in [0, 1]$.

Two Scenarios of the grading of the two basic component phases, ceramic and metal, through the wall thickness are considered.

Case (1): The phases vary symmetrically through the wall thickness, in the sense of having full ceramic at the outer surfaces of the plate and tending toward full metal at the mid-surface. For this case, $V_c(z)$ can be expressed as

$$V_c(z) = \left(\frac{z}{h/2}\right)^N \left(\frac{1+\operatorname{sgn}(z)}{2}\right) + \left(\frac{-z}{h/2}\right)^N \left(\frac{1-\operatorname{sgn}(z)}{2}\right), \tag{4}$$

where the Signum function is defined as

$$\operatorname{sgn}(z) = \begin{cases} 1, & \mathrm{z} > 0 \\ 0, & \mathrm{z} = 0 \\ -1, & \mathrm{z} < 0 \end{cases}. \tag{5}$$

N is termed the volume fraction index which provides the material variation profile through the plate wall thickness, $(0 \le N \le \infty)$. A pictorial representation of the distribution of the constituent materials are shown below in Fig. 2.

Case (2): The phases vary non-symmetrically through the wall thickness, and in this case there is full ceramic at the outer surface of the plate wall and full metal at its inner surface. For this case, $V_c(z)$ can be expressed as

$$V_c(z) = \left(\frac{h+2z}{2h}\right)^N . \tag{6}$$

Below is a pictorial representation of the antisymmetric case shown in Fig. 3.

It should be noted that in contrast to case (2), where there exists coupling between stretching and bending, such coupling is not present for the symmetric case (1). Also, for the purposes of simplicity the Poisson's ratio will be assumed to be constant throughout the plate structure. From Eqs. (1)-(6), the effective material properties of a FG plate can be expressed for the asymmetric case as

$$\left[E(z), \rho(z)\right] = (E_{cm}, \rho_{cm})\left(\frac{h+2z}{2h}\right)^N + (E_m, \rho_m) \tag{7}$$

and for the symmetric case as

$$\left[E(z), \rho(z)\right] = (E_{cm}, \rho_{cm})\left[\left(\frac{z}{h/2}\right)^N \left(\frac{1+\mathrm{sgn}(z)}{2}\right) + \left(\frac{-z}{h/2}\right)^N \left(\frac{1-\mathrm{sgn}(z)}{2}\right)\right] + (E_m, \rho_m) \tag{8}$$

$$\nu(z) = \nu , \tag{9}$$

Where

$$E_{cm} = E_c - E_m,\ \rho_{cm} = \rho_c - \rho_m. \tag{10}$$

3. KINEMATIC EQUATIONS

3.1 The 3-D Displacement Field

Consistent with the classical plate theory [6], the distribution of the 3-D displacement quantities through the wall thickness can be expressed as

$$u = u_0 - z w_{0,x}, \quad \upsilon = \upsilon_0 - z w_{0,y}, \quad w = w_0. \tag{11a-c}$$

Within these equations, (u, υ, w) are the 3-D displacement quantities along the (x, y, z) directions, respectively. While, u_0, υ_0, w_0 are the 2-D displacement quantities of the points on the mid-surface.

3.2 Non-Linear Strain-Displacement Relationships

The nonlinear strain displacement relationships across the plate thickness at a distance from the mid-surface take the form [2, 3, 6]

$$\varepsilon_{xx} = u_{,x} + w_{,x}^2/2, \; \varepsilon_{yy} = \upsilon_{,y} + w_{,y}^2/2, \; 2\varepsilon_{xy} = \gamma_{xy} = u_{,y} + \upsilon_{,x} + w_{,x}w_{,y}, \tag{12}$$

$$\varepsilon_{xz} = \varepsilon_{yz} = 0.$$

Substitution of Equations (11a-c) into Equations (12) results in the strain measures across the plate thickness in terms of the 2-D displacement quantities of the mid-surface of the plate expressed as

$$\begin{Bmatrix} \varepsilon_{xx} \\ \varepsilon_{yy} \\ \gamma_{xy} \end{Bmatrix} = \begin{Bmatrix} \varepsilon_{xx}^{(0)} \\ \varepsilon_{yy}^{(0)} \\ \gamma_{xy}^{(0)} \end{Bmatrix} + z \begin{Bmatrix} \varepsilon_{xx}^{(1)} \\ \varepsilon_{yy}^{(1)} \\ \gamma_{xy}^{(1)} \end{Bmatrix}, \tag{13}$$

Where

$$\{\varepsilon_{xx}^{(0)} \quad \varepsilon_{yy}^{(0)} \quad \gamma_{xy}^{(0)}\} = \{u_{,x} + w_{,x}^2/2 \quad \upsilon_{,y} + w_{,y}^2/2 \quad u_{,y} + \upsilon_{,x} + w_{,x}w_{,y}\} \tag{14a}$$

$$\{\varepsilon_{xx}^{(1)} \quad \varepsilon_{yy}^{(1)} \quad \gamma_{xy}^{(1)}\} = \{-w_{0,xx} \quad -w_{0,yy} \quad -2w_{0,xy}\}. \tag{14b}$$

In the above expressions, $(\varepsilon_{xx}^{0}, \varepsilon_{yy}^{0}, \gamma_{xy}^{0})$, are referred to as the membrane strains and $(\varepsilon_{xx}^{1}, \varepsilon_{yy}^{1}, \gamma_{xy}^{1})$ are referred to as the flexural bending strains which are also known as the curvatures.

4. CONSTITUTIVE EQUATIONS

The stress-strain relationships for a state of plane stress is expressed as [10]

$$\begin{Bmatrix} \sigma_{xx} \\ \sigma_{yy} \\ \sigma_{xy} \end{Bmatrix} = \begin{bmatrix} Q_{11} & Q_{12} & 0 \\ Q_{12} & Q_{22} & 0 \\ 0 & 0 & Q_{66} \end{bmatrix} \begin{Bmatrix} \varepsilon_{xx} \\ \varepsilon_{yy} \\ \gamma_{xy} \end{Bmatrix}$$

$$\sigma_{xz} = \sigma_{yz} = \sigma_{zz} = 0. \tag{15}$$

The material stiffnesses, $Q_{ij}(z), (i = 1,2,6)$ are given by [9, 10]

$$Q_{11} = Q_{22} = \frac{E(z)}{1-v^2},\ Q_{12} = \frac{vE(z)}{1-v^2},\ Q_{66} = \frac{E(z)}{2[1+v]},\ Q_{16} = Q_{26} = 0. \tag{16}$$

The standard force and moment resultants of a plate are defined as

$$(N_{ij}, M_{ij}) = \int_{-h/2}^{h/2} \sigma_{ij}(1, z)dz, \quad (i, j = x, y, xy). \tag{17}$$

With the use of Equations (12)–(17), the stress resultants and stress couples are related to the strains by [3]

$$\begin{Bmatrix} \{N\} \\ \{M\} \end{Bmatrix} = \begin{bmatrix} [A] & [B] \\ [B] & [D] \end{bmatrix} \begin{Bmatrix} \{\varepsilon^{(0)}\} \\ \{\varepsilon^{(1)}\} \end{Bmatrix}, \tag{18}$$

in which [A], [B], and [D] are the respective in-surface, bending-stretching coupling, and bending stiffnesses. For the case of symmetric FG Plates, [B]=0, since there is no bending-

stretching coupling. The global stiffness quantities, A_{ij}, B_{ij}, and D_{ij}, (i, j=1,2,6) are defined respectively as

$$(A_{ij}, B_{ij}, D_{ij}) = \int_{-h/2}^{h/2} Q_{ij}(1, z, z^2)dz\,. \tag{19}$$

In view of Equations (7), (8), (9), (16), and (19), the global stiffness quantities are determined as

$$[(A_{11}, A_{22}), (B_{11}, B_{22}), (D_{11}, D_{22})] = \frac{1}{1-\nu^2}(E_1, E_2, E_3)\,,$$

$$(A_{12}, B_{12}, D_{12}) = \frac{\nu}{1-\nu^2}(E_1, E_2, E_3)\,, \tag{20a-c}$$

$$(A_{66}, B_{66}, D_{66}) = \frac{1}{2(1+\nu)}(E_1, E_2, E_3),$$

where for the asymmetric case,

$$E_1 = E_{cm}h[1+1/(N+1)]\,,\quad E_2 = E_{cm}h^2[1/(N+2) - 1/(2N+2)] \tag{21}$$

$$E_3 = E_m h^3/12 + E_{cm}h^3[1/(N+3) - 1/(N+2) + 1/(4N+4)]$$

And for the symmetric case,

$$E_1 = E_{cm}h[1+1/(N+1)]\,,\; E_2 = 0\,,\; E_3 = E_{cm}h^3[1/12 + 1/4(N+3)]. \tag{22}$$

5. GOVERNING EQUATIONS

Hamilton's principle is used to derive the equations of motion and the boundary conditions. It is formulated as

$$\delta J = \delta \int_{t_0}^{t_1} (K - U + V)dt = 0\,, \tag{23}$$

where t_0 and t_1 are two arbitrary instants of time. U denotes the strain energy, V denotes the work done by surface tractions, edge loads, body forces, and viscous damping forces, and K denotes the kinetic energy of the 3-D body of the structure, while δ is the variational operator. In Equation (23), the strain energy is given by

$$\delta U = \int_{\Omega_0} \int_{-\frac{h}{2}}^{\frac{h}{2}} (\sigma_{xx}\delta\varepsilon_{xx} + \sigma_{yy}\delta\varepsilon_{yy} + \sigma_{xy}\delta\gamma_{xy}) dz d\Omega_0, \tag{24}$$

where Ω_0 denotes the mid-surface area of the panel. The work done by external loads is expressed as

$$\delta V = \int_{\Omega_0} [P_t(x,y,t) - 2\mu\dot{w}]\delta w d\Omega_0 + \int_x \int_{-\frac{h}{2}}^{\frac{h}{2}} \sigma_{yy}^* \delta v dz dx + \int_y \int_{-\frac{h}{2}}^{\frac{h}{2}} \sigma_{xx}^* \delta u dz dy. \tag{25}$$

In the above expression $P_t(x,y,t)$ is the transverse pressure, μ is the viscous damping coefficient per unit area of the plate, $(\sigma_{xx}^*, \sigma_{yy}^*)$ are the specified stress components along the plate edges, and $(\delta u, \delta v)$ are the virtual displacements in the normal and tangential directions, respectively, along the plate edges. Considering only the transversal inertia of the structure, the variation in kinetic energy is expressed as

$$\delta K = \int_{\Omega_0} I_0 \dot{w} \delta\dot{w} d\Omega_0, \tag{26}$$

where

$$I_0 = \int_{-\frac{h}{2}}^{\frac{h}{2}} \rho(z) dz, \tag{27}$$

and $\rho(z)$ is the mass per unit volume.

Considering Equation (23) in conjunction with Equations (24)-(27) , along with the constitutive equations (15), the strain-displacement relationships, equations (14), carrying out the integration through the thickness, integrating by parts whenever feasible, using the expression of global stress resultants and stress couples, while retaining only the transversal load, transverse inertia, and transverse damping, and invoking the arbitrary and independent character of variations $\delta u_0, \delta \upsilon_0, \delta w_0, \delta w_{0,x}, \delta w_{0,y}$, one obtains the equations of motion and as a by-product the boundary terms or conditions. This results in three equations of motion in terms of the global stress resultants and stress couples and four boundary conditions along the plate edges. These equations of motion and boundary conditions can be respectively expressed as

$$\delta u_0 : \quad N_{xx,x} + N_{xy,y} = 0 \tag{28}$$

$$\delta \upsilon_0 : \quad N_{yy,y} + N_{xy,x} = 0 \tag{29}$$

$$\delta w_0 : \quad \begin{aligned} & M_{xx,xx} + 2M_{xy,xy} + M_{yy,yy} + (N_{xx} w_{0,x} + N_{xy} w_{0,y})_x + (N_{yy} w_{0,y} + \\ & N_{xy} w_{0,x})_y + P_t - 2\mu \dot{w}_0 = I_0 \ddot{w}_0 \end{aligned} \tag{30}$$

The boundary conditions become

Along the edges $x = 0, L_1$

$$N_{xx} = 0 \quad \text{or} \quad u_0 = 0 \tag{31}$$

$$N_{xy} = 0 \quad \text{or} \quad \upsilon_0 = 0 \tag{32}$$

$$M_{xx} = 0 \quad \text{or} \quad w_{0,x} = 0 \tag{33}$$

$$M_{xx,x} + 2M_{xy,yy} + N_{xx} w_{0,x} + N_{xy} w_{0,y} = 0 \quad \text{or} \quad w_0 = 0 \tag{34}$$

Along the edges $y = 0, L_2$

$$N_{yx} = 0 \quad \text{or} \quad u_0 = 0 \tag{35}$$

$$N_{yy} = 0 \qquad \text{or} \qquad v_0 = 0 \tag{36}$$

$$M_{yy} = 0 \qquad \text{or} \qquad w_{0,y} = 0 \tag{37}$$

$$M_{yy,y} + 2M_{xy,xx} + N_{xy} w_{0,x} + N_{yy} w_{0,y} = 0 \qquad \text{or} \qquad w_0 = 0 \tag{38}$$

For the case of all edges simply supported and freely movable, the boundary conditions are as follows:

$$w_0 = M_{xx} = N_{xy} = 0, N_{xx} = N_{xx}^* \text{ on } x = 0, L_1 \tag{39}$$

$$w_0 = M_{yy} = N_{yx} = 0, N_{yy} = N_{yy}^* \text{ on } y = 0, L_2 \tag{40}$$

It should be mentioned for clarification sake that for compressive edge loading, $N_{xx}^* = -N_{xx}^0$, and $N_{yy}^* = -N_{yy}^0$.

AIR-BLAST LOADING

With the ever increasing demands for increased safety for the warfighter in the field to operate structurally sound vehicles in the event of an IED or some other type of explosive, it is imperative that an understanding of the structural response of various components within military combat vehicles under an explosive blast be understood so that measures can be taken from a design standpoint to ensure the durability and survivability of these components. To begin to achieve this understanding, the type of explosive loading considered here is a free in-air spherical air burst. Such an explosion creates a spherical shock wave which travels radially outward in all directions with diminishing velocity. The form of the incident blast wave from a spherical charge is shown in Fig. 4. Where P_{S0} is the peak overpressure above ambient pressure, P_0 is the ambient pressure, t_a is the time of arrival, t_p is the positive phase duration of the blast wave, and t is the time. The waveform shown in Fig. 4. is given by an expression known as the Friedlander equation and is given as

$$P_t(t) = (P_{S0} - P_0)[1-(t-t_a)/t_p]\exp[-\alpha(t-t_a)/t_p], \tag{41}$$

where

$$P_{S0} = 1772/Z^3 - 114/Z^2 + 108/Z. \tag{42}$$

In equations (41) and (42), Z is known as the scaled distance given by $Z = R/W^{1/3}$ with R being the standoff distance in meters and W being the equivalent charge weight of TNT in terms of kilograms. Also, α is known as the decay parameter which is determined by adjustment to a pressure curve from a blast test.

For the conditions of standard temperature and pressure (STP) at sea level, the time of arrival t_a and the positive phase duration t_p can be determined from [5]

$$t/t_1 = R/R_1 = (W/W_1)^{1/3}. \tag{43}$$

t_1 represents either the arrival time or positive phase duration for a reference explosion of charge weight W_1, and t represents either the arrival time or positive phase duration for any explosion of charge weight W. The determination of the standoff distance for any charge weight W follows a similar reasoning. The application of these relationships is known as cube root scaling. It should be understood that in applying these relationships that the standoff distances are themselves scaled according to the cube root law.

6. SOLUTION METHODOLOGY

To satisfy the first two equations of motion, equations (28,29), a stress potential will be utilized which allows the in-plane stress resultants to be expressed by letting

$$N_{xx} = \varphi_{,yy}, N_{yy} = \varphi_{,xx}, N_{xy} = -\varphi_{,xy}. \tag{44}$$

The third equation of motion, equation (30), can be expressed in terms of two unknown variables, the stress potential φ and the transverse displacement w_0. To accomplish this, a partial inversion, of equation (18), the details of which are not presented here, needs to be carried out. Performing a partial inversion results in [4]

$$\begin{Bmatrix} \{\varepsilon^{(0)}\} \\ \{M\} \end{Bmatrix} = \begin{bmatrix} [A^*] & [B^*] \\ -[B^*]^T & [D^*] \end{bmatrix} \begin{Bmatrix} \{N\} \\ \{\varepsilon^{(1)}\} \end{Bmatrix}, \tag{45}$$

where

$$[A^*] = [A]^{-1}, \ \ [B^*] = -[A]^{-1}[B] \ \ , \ -[B^*]^T = [B][A]^{-1}$$

$$[D^*] = [D] - [B][A]^{-1}[B]. \tag{46}$$

Using Equations (44), (45), and (46) and simplifying, equation (30) takes the form

$$D\nabla^4 w_0 - (\varphi_{,xx} w_{0,yy} - 2\varphi_{,xy} w_{0,xy} + \varphi_{,yy} w_{0,xx}) + I_0 \ddot{w}_0 + 2\mu \dot{w}_0 = P_t \tag{47a}$$

where

$$D = \frac{E_1 E_3 - E_2^2}{E_1(1-\nu^2)}, \quad \theta = -\frac{E_2}{E_1}. \tag{47b,c}$$

This gives one governing equation with two unknowns, w_0 and φ. One more equation is needed in terms of the same unknowns which will give two equations in terms of two unknowns which can then be solved. This will come from the compatibility equation. By eliminating the in-plane displacements from the strain-displacement relationships, equations (14) the relationship between the in-plane strains and the transversal deflection known as the compatibility equation can be shown to be given by

$$\varepsilon^0_{xx,yy} + \varepsilon^0_{yy,xx} - \gamma^0_{xy,xy} = w^2_{0,xy} - w_{0,xx} w_{0,yy}. \tag{48}$$

In view of equations (44) , (45), and (46), the compatibility equation is expressed as

$$\nabla^4 \varphi = E_1 (w_{0,xy} - w_{0,xx} w_{0,yy}). \tag{49}$$

In equations (47a) and (49), $\nabla^2 = \partial^2/\partial x^2 + \partial^2/\partial y^2$ where ∇ is referred to as the Laplacian operator.

Equations (47a) and (49) are the basic governing equations used to investigate the structural response of FG plates under external excitation loading. For the purposes of this paper, from this point forward, the thermal terms will be discarded. To this end, to solve equations (47a) and (49), the approach adopted from [2] will be utilized. In this respect, the following functional forms are assumed for w_0 and φ [2].

$$w_0(x, y, t) = w_{mn}(t) \sin \lambda_m x \sin \mu_n y$$

$$\begin{aligned} \varphi(x, y, t) = A_{mn}(t) \cos 2\lambda_m x + B_{mn}(t) \cos 2\mu_n y + C_{mn}(t) \cos 2\lambda_m x \cos 2\mu_n y + \\ D_{mn}(t) \sin \lambda_m x \sin \mu_n y + \frac{1}{2} N_{xx}^* y^2 + \frac{1}{2} N_{yy}^* x^2, \end{aligned} \tag{50a,b}$$

where $\lambda_m = m\pi / L_1$, $\mu_n = n\pi / L_2$, $m, n = 1,2,...$ are the number of half waves in the x and y directions, respectively, and $w_{mn}(t)$ is the amplitude of deflection. Also, $A_{mn}(t)$, $B_{mn}(t)$, $C_{mn}(t)$, and $D_{mn}(t)$ are coefficients to be determined. By substituting equations (50a,b) into equation (49), the coefficients $A_{mn}(t)$, $B_{mn}(t)$, $C_{mn}(t)$, and $D_{mn}(t)$ are determined as

$$A_{mn}(t) = E_1 w_{mn}^2(t) \mu_n^2 / 32\lambda_m^2, \quad B_{mn}(t) = E_1 w_{mn}^2(t) \lambda_m^2 / 32\mu_n^2, \quad C_{mn}(t) = D_{mn}(t) = 0. \tag{51}$$

As a result of the assumed form for the Airy's potential function, φ the following relationships expressed mathematically as

$$\int_0^{L_2} \varphi_{,yy}\Big|_{x=0, L_1} dy = N_{xx}^* L_2, \quad \int_0^{L_1} \varphi_{,xx}\Big|_{y=0, L_2} dx = N_{yy}^* L_1, \tag{52}$$

implies that N_{11}^*, N_{22}^* acquire the meaning of average in-plane compressive edge loads. Moreover, by assuming

$$P_t(x,y,t) = P_{mn}(t)\sin\lambda_m x\sin\mu_n y, \tag{53a}$$

which implies through integration of both sides over the plate area that

$$P_{mn}(t) = \frac{4}{L_1 L_2}\int_0^{L_2}\int_0^{L_1} P_t(x,y,t)\sin\lambda_m x\sin\mu_n y dxdy\,. \tag{53b}$$

Letting,

$$P_t(x,y,t) = P_t(t) = (P_{S0} - P_0)[1-(t-t_a)/t_p]\exp[-\alpha(t-t_a)/t_p] \tag{53c}$$

and integrating gives

$$P_{mn}(t) = 16P_t(t)/\pi^2. \qquad (m,n) = (1,1) \tag{53d}$$

Introduction of equations (50a,b) and (51) into equation (47a) and retaining the resulting equation along with the unsatisfied boundary conditions in the energy functional and applying the Extended Galerkin technique results in the following ordinary nonlinear differential equation governing the structural response of FG plates, under external excitation which is expressed as

$$\ddot{w}_{mn}(t) + 2\Delta_{mn}\omega_{mn}\dot{w}_{mn}(t) + \omega_{mn}^2 w_{mn}(t) + \Omega_{mn}(t)w_{mn}^3(t) = \widetilde{P}_{mn}(t), \tag{54}$$

where $w_{mn}(t)$ represents the amplitude of deflection of the plate as a function of time, $\widetilde{P}_{mn}(t) = 16P_t(t)/I_0\pi^2$, $\omega_{mn} = \sqrt{K_{mn}/I_0}$ is the natural frequency of the FG plate, $\Delta_{mn} = \mu/I_0\omega_{mn}$ is the non-dimensional damping factor, and $\Omega_{mn} = E_1(\lambda_m^4 + \mu_n^4)/16I_0$. It should be noted that at the center of the plate $(x,y) = (L_1/2, L_2/2)$, $w_{mn}(t)$ is equal to the maximum deflection of the plate. In these latter expressions,

$$K_{mn} = D(\lambda_m^2 + \mu_n^2)^2 + N_{xx}^*\lambda_m^2 + N_{yy}^*\mu_n^2\,. \tag{55}$$

Equation (54) is a nonlinear equation in terms of the plate deflections as a function of time. It is interesting to note that equation (54) is very similiar to Duffing's Equation. To obtain the plate deflections as a function of time, equation (54) is solved using the Fourth-Order Runge-Kutta Method with zero initial conditions.

6.1 Special Case – Constant Uniform distributed Transverse Pressure

For validation purposes later on, the special case of a constant uniformly distributed transverse pressure acting on the top surface of the plate, independent of time, for a square plate will be shown [1]. For a square plate under a uniform pressure independent of time, $\ddot{w}_{mn}(t) = 0$, and $\dot{w}_{mn}(t) = 0$. As a result, equation (54) reduces to

$$\omega_{mn}^2 w_{mn} + \Omega_{mn} w_{mn}^3 = \widetilde{P}_{mn}. \tag{56}$$

Neglecting tensile or compressive loading, equation (56) can be written as

$$\frac{E_1}{16}(\lambda_m^4 + \mu_n^4) w_{mn}^3 + D(\lambda_m^2 + \mu_n^2)^2 w_{mn} = \widetilde{P}_{mn} \tag{57}$$

Where,

$$\widetilde{P}_{mn} = \frac{16 P_t}{mn\pi^2}. \tag{58}$$

Equation (57) is a nonlinear algebraic equation which can be solved by a typical numerical technique for the load-deflection relationship. This will be shown graphically in the results section.

7. ELASTIC STRESS ANALYSIS

With the transversal deflections in hand, as a function of time, and with the use of equations (13), (14a,b), (15), and (16), the constitutive equations become

$$\sigma_{xx}(x, y, z, t) = \frac{E(z)}{1-v^2}\left[u_{0,x} + \frac{1}{2}w_{0,x}^2 + v\left(v_{0,y} + \frac{1}{2}w_{0,y}^2\right) - z(w_{0,xx} + v w_{0,yy})\right]$$

$$\sigma_{yy}(x,y,z,t) = \frac{E(z)}{1-v^2}\left[v_{0,y} + \frac{1}{2}w_{0,y}^2 + v\left(u_{0,x} + \frac{1}{2}w_{0,x}^2\right) - z(w_{0,yy} + vw_{0,xx})\right]$$

$$\sigma_{xy}(x,y,z,t) = \frac{E(z)}{2(1+v)}\left[u_{0,y} + v_{0,x} + w_{0,x}w_{0,y} - 2zw_{0,xy}\right]. \tag{59a-c}$$

At this point, all thermal terms have been discarded since the thermal response is not the subject of this paper. In order to determine the stresses, the expressions for u_0 and v_0 in terms of the transversal amplitude of deflection, $w_{mn}(t)$ needs to be determined. These relationships can be determined from the global constitutive equations (18). Expanding equation (18) gives,

$$N_{xx} = A_{11}\varepsilon_{xx}^{(0)} + A_{12}\varepsilon_{yy}^{(0)} + B_{11}\varepsilon_{xx}^{(1)} + B_{12}\varepsilon_{yy}^{(1)}$$

$$N_{yy} = A_{12}\varepsilon_{xx}^{(0)} + A_{22}\varepsilon_{yy}^{(0)} + B_{12}\varepsilon_{xx}^{(1)} + B_{22}\varepsilon_{yy}^{(1)}. \tag{60a,b}$$

Solving equations (60a,b) simultaneously for $\varepsilon_{xx}^{(0)}$, and $\varepsilon_{yy}^{(0)}$ in terms of N_{xx}, N_{yy}, $\varepsilon_{xx}^{(1)}$, and $\varepsilon_{yy}^{(1)}$ and utilizing equations (14) and (44) gives,

$$u_{0,x} = \frac{1}{E_1}(\varphi_{,yy} - v\varphi_{,xx}) + \frac{E_2}{E_1}w_{0,xx} - \frac{1}{2}w_{0,x}^2$$

$$v_{0,y} = \frac{1}{E_1}(\varphi_{,xx} - v\varphi_{,yy}) + \frac{E_2}{E_1}w_{0,yy} - \frac{1}{2}w_{0,y}^2. \tag{61a,b}$$

With the use of equations (20a-c), (50a,b), and (51), and integrating results in,

$$u_0 = \frac{-w_{mn}^2(t)\lambda_m^2}{8}x - \frac{w_{mn}^2(t)\mu_n^2}{16\lambda_m}\sin 2\lambda_m x\left(\frac{2\lambda_m^2}{\mu_n^2}\sin^2\mu_n y - v\right) + \frac{w_{mn}(t)E_2\lambda_m}{E_1}\cos\lambda_m x\sin\mu_n y$$
$$+\frac{1}{E_1}(N_{xx}^* - vN_{yy}^*)x + C_1$$

$$v_0 = \frac{-w_{mn}^2(t)\mu_n^2}{8} y - \frac{w_{mn}^2(t)\lambda_m^2}{16\mu_n} \sin 2\mu_n y \left(\frac{2\mu_n^2}{\lambda_m^2} \sin^2 \lambda_m x - v \right) + \frac{w_{mn}(t) E_2 \mu_n}{E_1} \sin \lambda_m x \cos \mu_n y$$
$$+ \frac{1}{E_1}(N_{yy}^* - vN_{xx}^*) y + C_2$$

(62a,b)

Finally, substitution of equation (50a), and equations (62a,b) into equations (59a-c) gives the expressions of the stresses as,

$$\sigma_{xx}(x,y,z,t) = -\frac{E(z)}{1-v^2} \left\{ \frac{(1-v^2)\lambda_m^2}{8} w_{mn}^2(t) \cos 2\mu_n y - \left(z - \frac{E_2}{E_1} \right) \left(\lambda_m^2 + v\mu_n^2 \right) w_{mn}(t) \sin \lambda_m x \sin \mu_n y \right.$$
$$\left. + \overline{N}_{xx} \right\}$$

$$\sigma_{yy}(x,y,z,t) = -\frac{E(z)}{1-v^2} \left\{ \frac{(1-v^2)\mu_n^2}{8} w_{mn}^2(t) \cos 2\lambda_m x - \left(z - \frac{E_2}{E_1} \right) \left(\mu_n^2 + v\lambda_m^2 \right) w_{mn}(t) \sin \lambda_m x \sin \mu_n y \right.$$
$$\left. + \overline{N}_{yy} \right\}$$

$$\sigma_{xy}(x,y,z,t) = -\frac{E(z)}{1+v} \left\{ \left(z - \frac{E_2}{E_1} \right) \lambda_m \mu_n w_{mn}(t) \cos \lambda_m x \cos \mu_n y \right\}. \qquad (63a\text{-}c)$$

Where,

$$\overline{N}_{xx} = \frac{(1-v^2)N_{xx}^0}{E_1}, \ \overline{N}_{yy} = \frac{(1-v^2)N_{yy}^0}{E_1} \qquad (64a,b)$$

are the nondimensional compressive edge loadings.

7.1 Special Case – Constant Uniformly Distributed Transverse Pressure

Under the same assumptions used in section 6.1, the in plane axial stress, σ_{xx}, is given as

$$\sigma_{xx} = \frac{E(z)}{1-v^2} \left\{ \left(\frac{(1-v^2)\lambda_m^2}{8} \right) w_{mn}^2 + \left(z - \frac{E_2}{E_1} \right) (\lambda_m^2 + v\mu_n^2) w_{mn} \right\}. \qquad (65)$$

It should be mentioned that for a square plate, $\sigma_{xx} = \sigma_{yy}$. Also, $\sigma_{xy} = 0$ at the center of the plate. Once the deflections are determined from equation (57), they are then substituted into equation (65) to determine the load-stress relationship. This will be shown graphically in the results section.

8. RESULTS AND DISCUSSION

To validate the present theory, comparisons are made with Woo and Meguid [1] who considered a transverse uniform pressure, independent of time, acting on the surface of asymmetric functionally graded (FG) plates and shallow shells. Figures 5 and 6 show comparisons between the present results and Woo and Meguid. The geometrical and material properties used for the comparison are given as

$$L_1 = 0.2\, m, \qquad h = 0.01\, m, \qquad \psi = 1$$

$$\text{Aluminum}: \ E_m = 70\, GPa, \qquad \nu = 0.3$$

$$\text{Alumina}: \ E_c = 380\, GPa, \qquad \nu = 0.3\,.$$

Figure 5 reflects the relationship between the dimensionless central deflection and the load parameter $Q = P_t L_1^4 / E_m h^4$. Inspection of both results (Present and Woo and Meguid) reveals somewhat of a marginal difference. This marginal difference seems to increase as the load parameter Q becomes larger. Also the differences appear larger for pure metal (Aluminum) as opposed to pure ceramic (Alumina). In both cases, with larger deflections, comes larger differences. The differences, most likely come from the fact that Woo and Meguid assumed a different solution process which consisted of a combination of series solutions and or Fourier series representations, for their deflection profile, in combination with numerical methods. For the present solution process, a one term Navier type solution was utilized for the deflection profile. In addition, the Galerkin Method which is an approximate method was used to facilitate

the governing equation with was then solved using the Runge-Kutta mathod. Two different solution processes were utilized between the present author and Woo and Meguid.

Figure 6 highlights the relationship between the dimensionless axial stress $\sigma = \sigma_x L_1^2 / E_m h^2$ and the dimensionless thickness $\zeta = z/h$ for a fixed value for the load parameter Q = -400. Since there are differences existing with the deflection-load history, their will be differences revealed with the stress distribution. By observation, it can be seen that some marginal differences exist. Again, this is attributed to the fact that two unrelated approaches were utilized to arrive at the same final results.

To illustrate the present approach, a ceramic-metal functionally graded plate consisting of Ti-6Al-4V and Aluminum Oxide, with the following material properties, were considered for the numerical results presented.

$$E_c = 320.24\,\text{GPa}, \quad \rho_c = 3750\,\text{kg}/m^3, \quad v_c = 0.26$$
$$E_m = 105.7\,\text{GPa}, \quad \rho_m = 4429\,\text{kg}/m^3, \quad v_m = 0.2981$$
$$v_{ave} = 0.2791$$

The geometrical properties used for the FG Plate are $L_1 = 1\,\text{m}$, $\psi = L_1/L_2 = 1$, and unless otherwise stated $h = 0.0254\,\text{m}$, the decay factor, $\alpha = 0.5$, and the halfwaves, (m,n) = (1,1). In addition, the following reference values, in Table 1, were utilized to determine the time of arrival and positive phase duration [5].

Figure 7 depicts the central 2-D stress-time history of an asymmetric FG plate, on the top surface of the plate, with damping and an aspect ratio of 1.25. both stress-time histories have the same frequency but different amplitudes. It is revealed that for aspect ratios greater than one σ_{yy} has larger amplitudes. Although not shown here, when the aspect ratio is equal to 1, the stress-

time history for σ_{xx}, σ_{yy} are the same (same frequency and amplitudes). When the aspect ratio is less than 1, the amplitudes of the stress-time history of σ_{xx} is larger than for σ_{yy} with identical frequencies. In Figure 8, the central stress-time histories of the stress component, σ_{xx} on the top surface of the plate, for various volume fraction indexes, is depicted. Three comparisons are made between fully ceramic, fully metal, and FG with ceramic and metal. As the plate construction transforms from fully ceramic to fully metal, it does so with decreasing frequency and increased stress amplitude. In other words, the fully ceramic case has the highest frequency due to its increased stiffness but with a lower stress amplitude. In contrast the fully metal case has the highest stress amplitude and the lowest frequency due to its decreased stiffness when compared with ceramic. This figure shows that for some applications ceramic may be more beneficial to adopt. Figure 9 depicts the damped stress-time histories, of an asymmetric plate, for the 2-D stress component, σ_{xx} at three different central locations which include the top surface, the middle surface, and the bottom surface. It can be seen that on the central top surface (ceramic) the stress-time history starts out in compression along with the top surface in tension. It is also revealed that the central stress amplitude on the top surface (ceramic) is larger than for the bottom surface (metal). The ceramic bears a large portion of the stress since the ceramic acts as a restraint in preventing the metal surface from a large amount of deformation and or stress build-up. The central stress-time history for the middle surface is very small in amplitude, although not zero (not a neutral surface). Figure 10 is the counterpart of figure 9 for the case of a symmetric FG plate with ceramic on the top and the bottom surface with metal in between. It can be seen that the central stress-time histories for both the top and bottom surfaces are almost reflections of one another. Both have the same frequency but are out of phase with each other. Although almost symmetrical, it should be noted that the stress on the middle surface is not zero

in contrast to beam theory. the middle surface is not a neutral surface but very close. The stress-time history is negligible when compared to the top and bottom surfaces. Figure 11 compares the central stress-time history for σ_{xx} on the bottom surface for both the asymmetric and symmetric FG constructions. While both histories exhibit the similar behavior, the symmetric case generates larger amplitudes when it is in both compression and tension. The plausible explanation for this behavior is that both ceramic surfaces which by nature are stiffer than the middle surface being metal act as a constraint preventing the metal from an attributable amount of deformation. The ceramic bears most of the stress with little deformation. Figure 12 is the counterpart of figure 11 comparing the symmetries at the middle surface. Again although the stress profiles are small they are not zero. The middle surface is not a neutral surface. Finally, in figure 13, which is the counterpart of both figures 11 and 12 at the top surface of the plate, it is shown that there is only a negligible difference in the central stress-time histories between the asymmteric and symmetric case. It appears that in both cases the ceramic bears the same amount of stress irrespective of the symmetry.

As a final point of discussion, a comment or two should be made about permanent deformation and fracture. The theory presented here is based on elasticity theory which does not take plastic deformation or fracture into account. It is assumed that the behavior of the plate remains within the elastic limit. To determine if the elastic limit is exceeded by way of deformation or induced stresses, appropriate verification and validation (V&V) would need to be carried out through laboratory testing per the required material phase (ceramic and metal) distribution throughout the structure. Another option includes (V&V) against finite element modeling and simulation (M&S) software which may include a more accurate material model

such as the Johnson-Cook material model based on a high strain-rate of behavior of loading which is not captured in the elasticity theory.

9. CONCLUDING REMARKS

A rigorous treatment of functionally graded plates with grading in the transverse direction for two different types of functionally graded symmetries (asymmetric and symmetric) has been studied. Validations with a simpler case consisting of a transverse uniform load found in Woo and Meguid [1], has been made. It has been shown that damping has an important effect when it comes to the attenuation of the deflections. It has also been shown that other factors such as the magnitude of the volume fraction index, the aspect ratio, the location of the stress, and most importantly, the symmetry of the transverse grading throughout the structure plays an important role in the central stress-time history of the structure.

It has also been shown that the ceramic carries a large part of the axial stress while acting as a constraint in the deformation of the metallic phase. Also, the neutral surface does not reside in the middle surface of the plate. In addition, it is apparent that the stress-time history of the metallic phase exhibits larger amplitudes of stress but lower frequencies in contrast to ceramic which exhibits the opposite behavior due to its stiffness.

From a design standpoint, depending on the design requirements, it would be appropriate to state that integration of FG materials in plate-type structures would benefit the structure response of the structure. It is hoped and realized that this present study presented here will give insight into some of the factors that can play an important role in the structural response of functionally graded plates and fill in some of the fundamental missing gaps within this subject area.

UNCLASSIFIED: Dist A. Approved for public release

ACKNOWLEDGEMENTS

The author would like to express his thanks to the U.S. Army-RDECOM-TARDEC for their support and funding under the Independent Laboratory In-house Research program (ILIR).

REFERENCES

[1] J. Woo and S.A. Meguid, "Nonlinear Analysis of Functionally Graded Plates and Shallow Shells", *International Journal of Solids and Structures*, Vol 38, Pgs. 7409-7421, 2001.

[2] Hoang Van Tung and Nguyen Dinh Duc, "Nonlinear Analysis of Stability for Functionally Graded Plates Under Mechanical and Thermal Loads", *Composite Structures*, Vol 92, Pgs. 1184-1191, 2010.

[3] Hui-Shen Shen, "Functionally Graded Materials-Nonlinear Analysis of Plates and Shells" *CRC Press*, 2009.

[4] Hui-Shen Shen, "Karman-Type Equations for a Higher-Order Shear Deformation Plate Theory and its Use in the Thermal Postbuckling Analysis", *Applied Mathematics and Mechanics*, (English Edition, Vol. 18, No.12, Dec 1997).

[5] Kingery, C.N. and G. Bulmash, "Air-Blast Parameters from TNT Spherical Airburst and Hemispherical Surface Burst", ABRL-TR-02555, U.S. Army Ballistic Research Laboratory, Aberdeen Proving Ground, MD, April 1984.

[6] Reddy, J.N., "Mechanics of Laminated Composite Plates and Shells - Theory and Analysis", 2^{nd} Edition, *CRC Press*, 1997.

FIGURE CAPTIONS

Fig 1. A simply supported functionally graded plate shown in 2-D under an explosive blast.

Fig 2. Distribution of the constituent materials through the plate thickness for the symmetric case.

Fig 3. Distribution of the constituent materials through the plate thickness for the antisymmetric case.

Fig 4. Incident pressure profile of a blast wave.

Fig 5. Validation of the dimensionless central deflection versus uniform transverse load.

Fig 6. Validation of the dimensionless axial stress along the thickness z at the center of the plate under the load parameter Q = -400

Fig 7. 2D stress components versus time for an asymmetric FG plate (N=0.5).

Fig 8. The axial stress component along the x direction versus time for various values of the volume fraction index.

Fig 9. The axial stress component along the x direction versus time at various locations throughout the thickness at the center of the plate for an asymmetric FG Plate (N=0.5).

Fig 10. The counterpart of figure 9 for a symmetric FG plate (N=0.5).

Fig 11. The axial stress component along the x direction versus time for both the asymmetric and symmetric FG plate on the bottom surface at the center of the plate (N=0.5).

Fig 12. The axial stress component along the x direction versus time for both the asymmetric and symmetric FG plate on the middle surface at the center of the plate (N=0.5).

Fig 13. The axial stress component along the x direction versus time for both the asymmetric and symmetric FG plate on the top surface at the center of the plate (N=0.5).

TABLES

Table 1. Airblast Parameters Versus Distance for a One Kilogram (W_1) TNT Spherical Air Burst [5].

Standoff Distance, R_1 (m)	Arrival Time, t_{a_1} (msec)	Positive Phase Duration, t_{p_1} (msec)
1.0	0.532	1.79

FIGURES (In Numerical order)

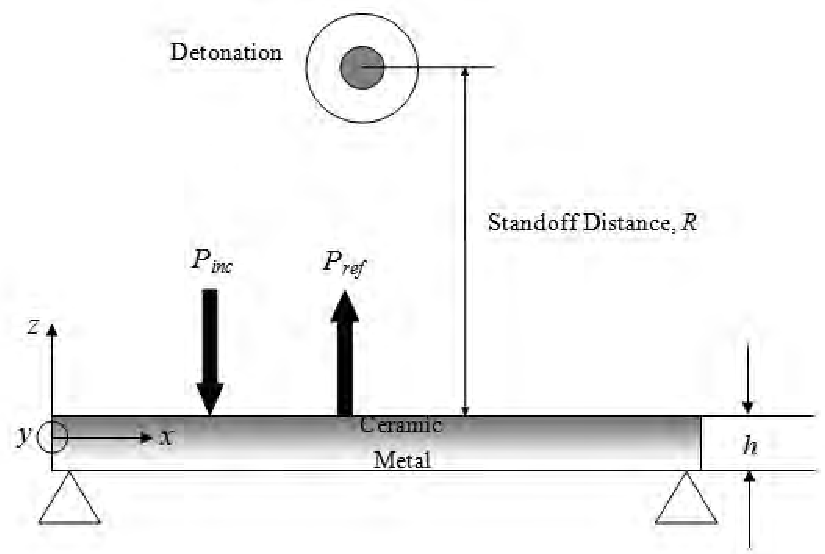

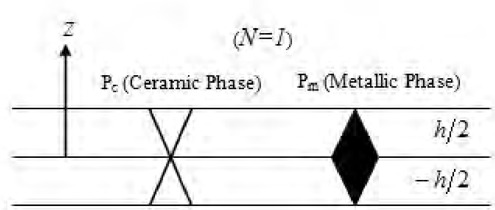

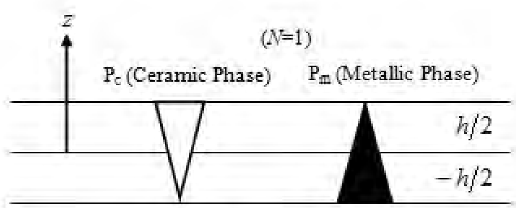

UNCLASSIFIED: Dist A. Approved for public release

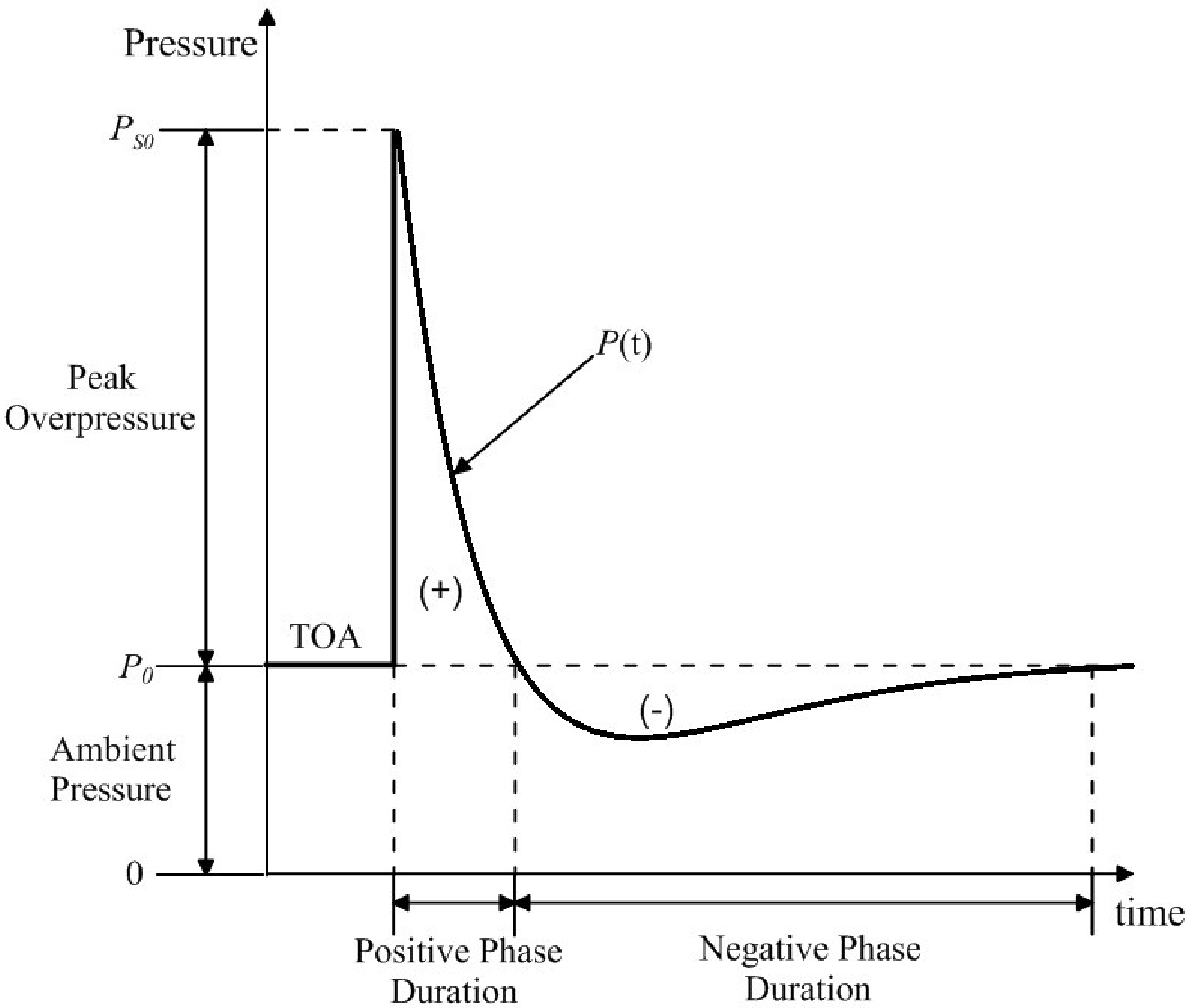
Pressure
P_{S0}
Peak
Overpressure
$P(t)$
(+)
TOA
P_0
(-)
Ambient
Pressure
0
time
Positive Phase
Duration
Negative Phase
Duration

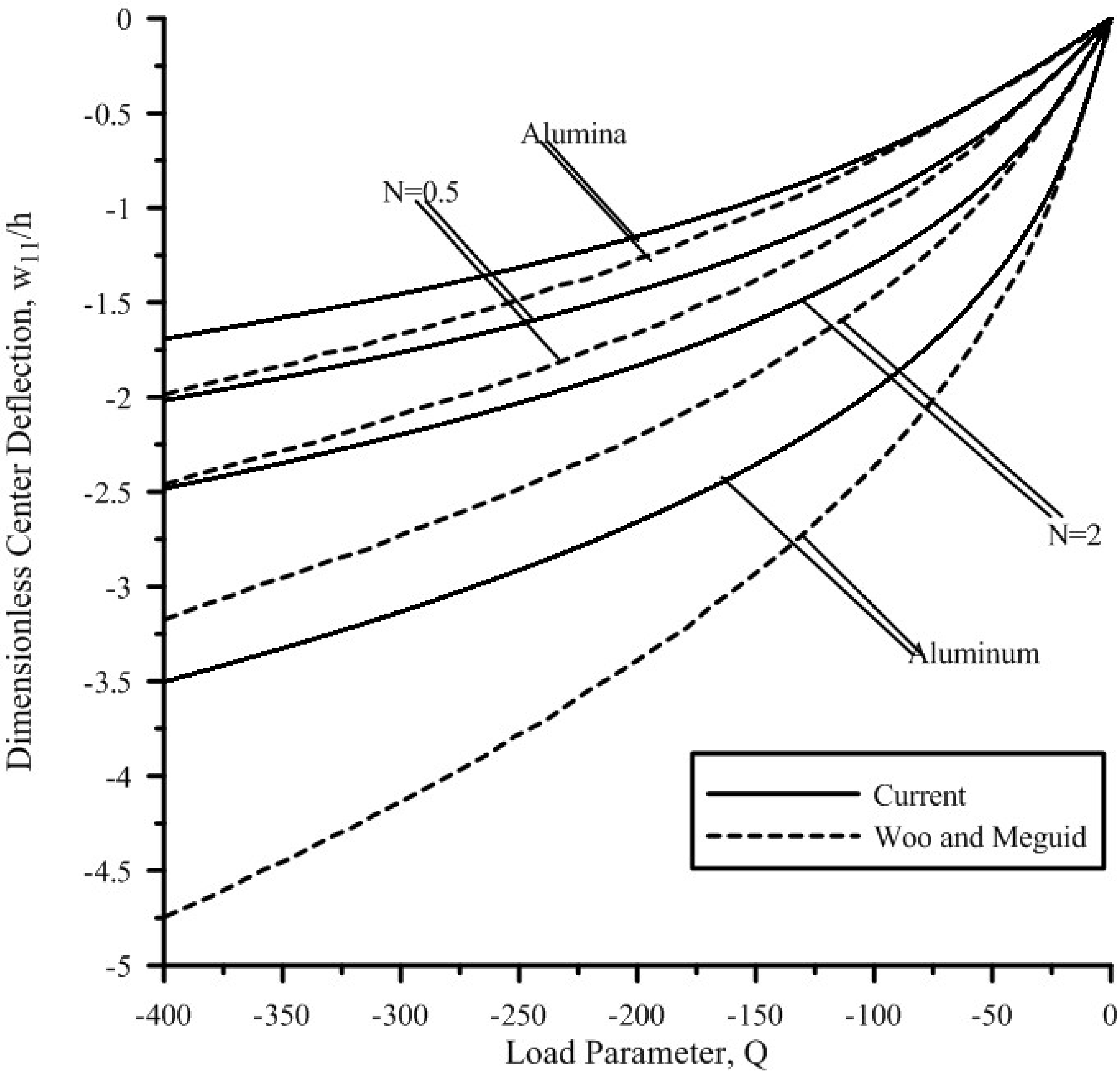

Dimensionless Center Deflection, w_{11}/h
Load Parameter, Q
0
-0.5
-1
-1.5
-2
-2.5
-3
-3.5
-4
-4.5
-5
-400
-350
-300
-250
-200
-150
-100
-50
0
Alumina
N=0.5
N=2
Aluminum
Current
Woo and Meguid

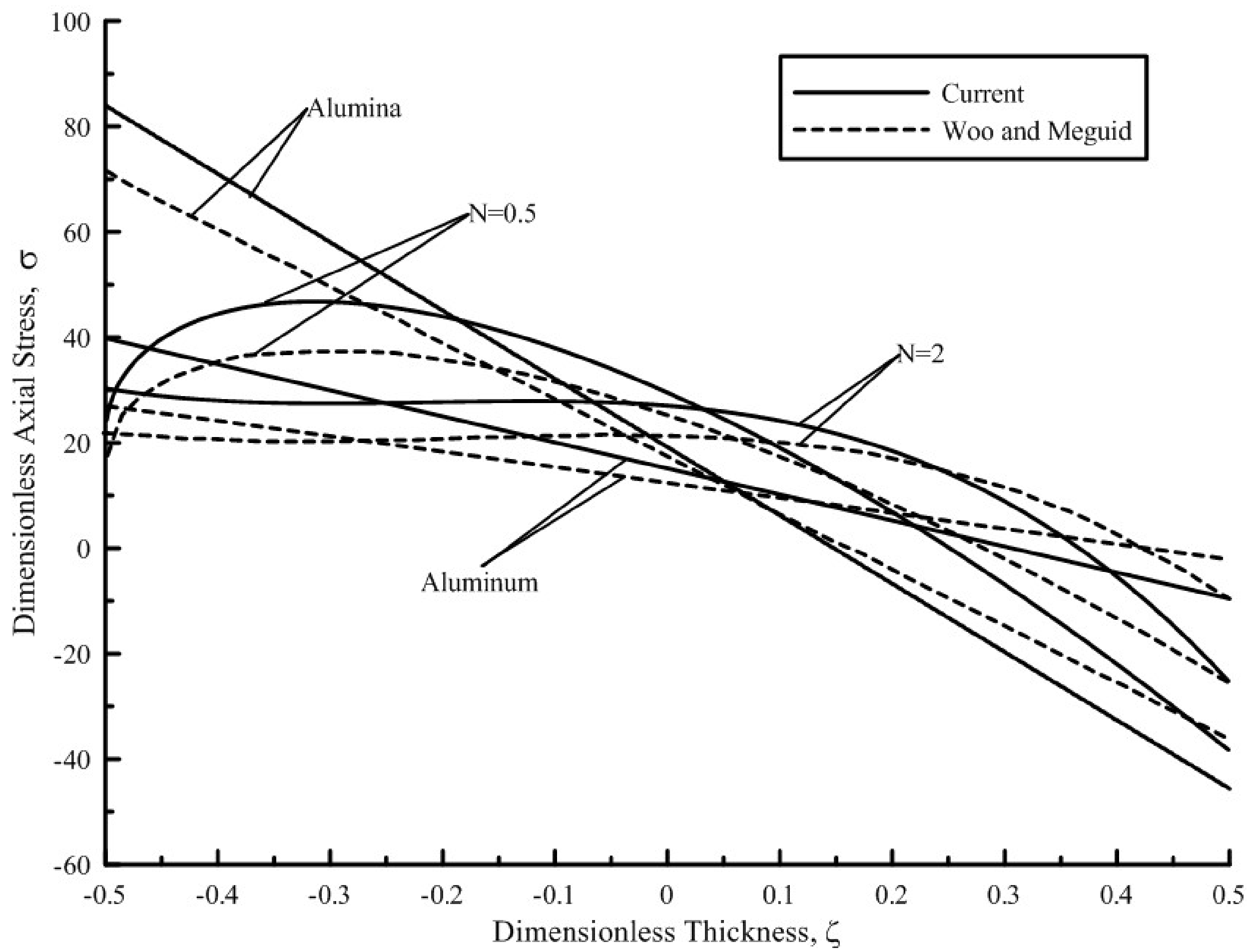
100
80
60
40
20
0
-20
-40
-60
Dimensionless Axial Stress, σ
-0.5
-0.4
-0.3
-0.2
-0.1
0
0.1
0.2
0.3
0.4
0.5
Dimensionless Thickness, ζ
Current
Woo and Meguid
Alumina
N=0.5
N=2
Aluminum

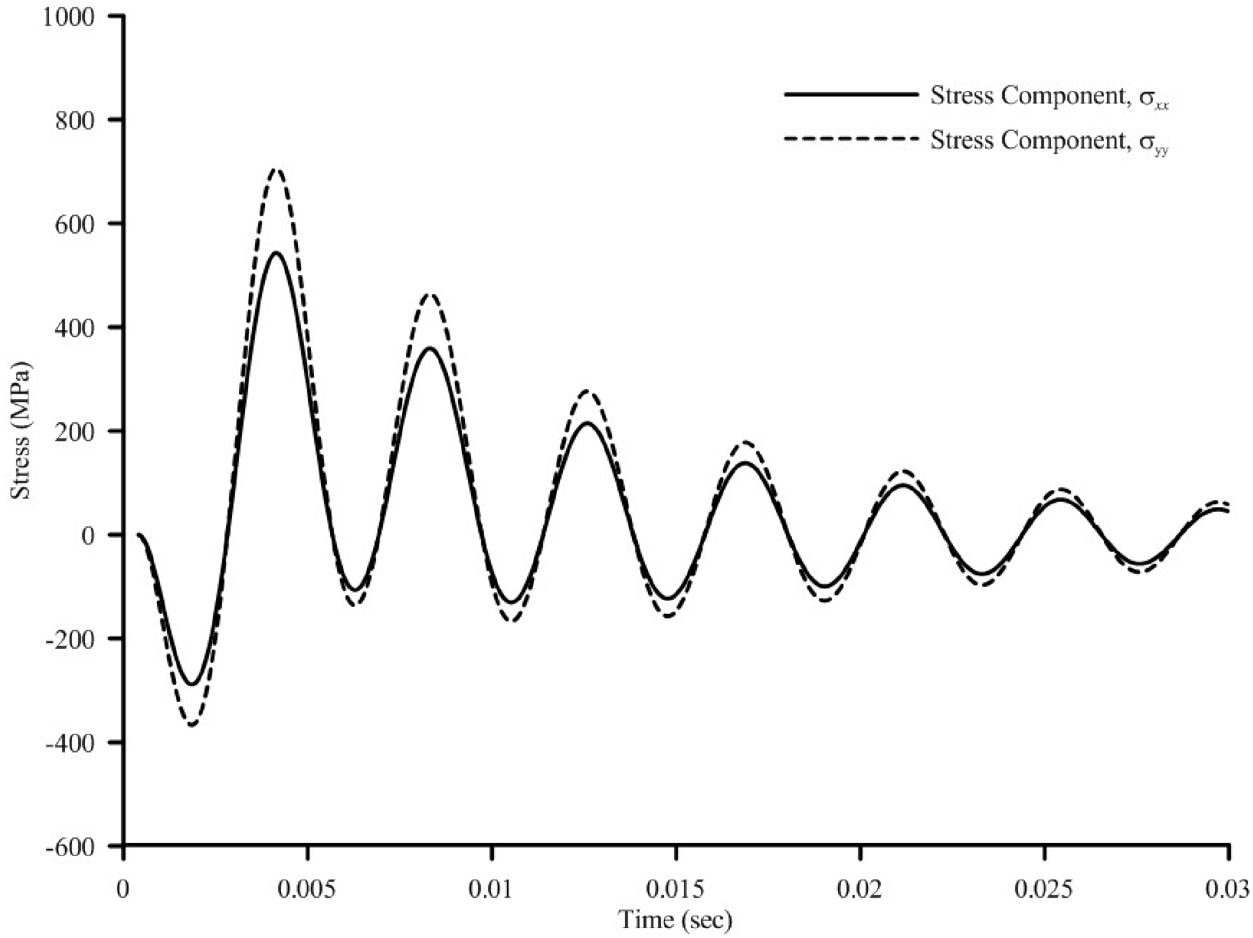

Stress Component, σ_{xx}
Stress Component, σ_{yy}
Stress (MPa)
1000
800
600
400
200
0
-200
-400
-600
0
0.005
0.01
0.015
0.02
0.025
0.03
Time (sec)

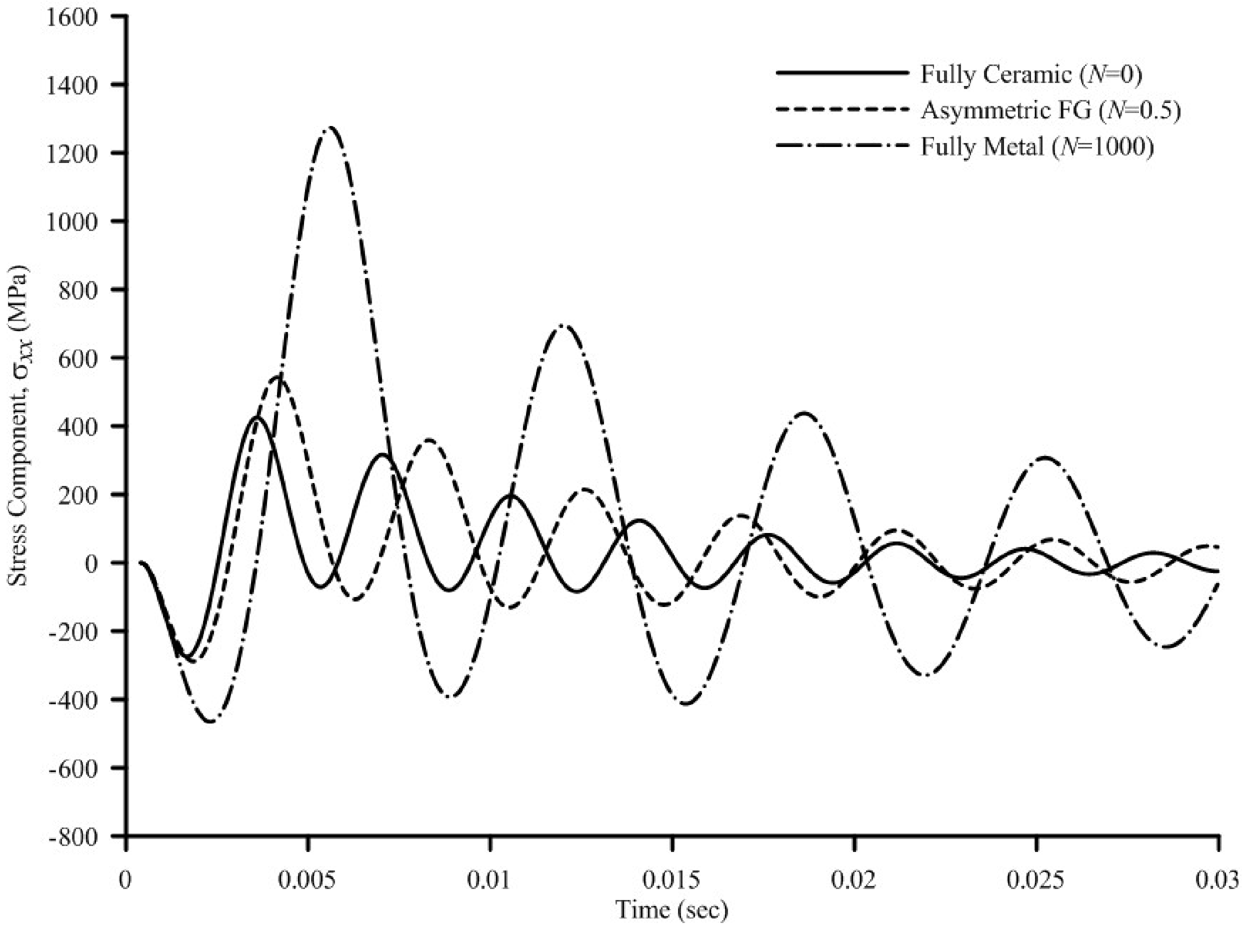
Fully Ceramic (N=0)
Asymmetric FG (N=0.5)
Fully Metal (N=1000)
Stress Component, σxx (MPa)
Time (sec)
1600
1400
1200
1000
800
600
400
200
0
-200
-400
-600
-800
0
0.005
0.01
0.015
0.02
0.025
0.03

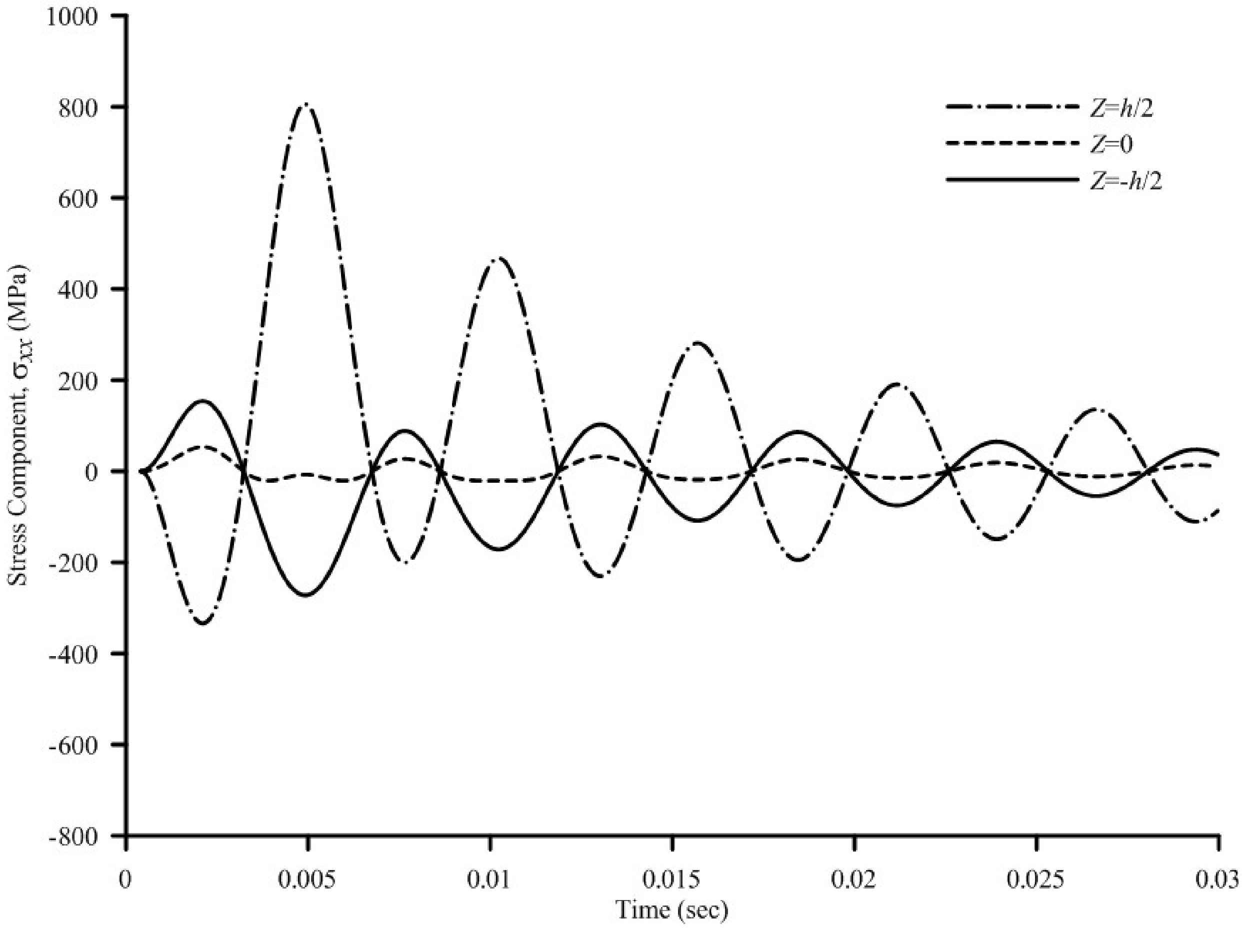
1000
800
600
400
200
0
-200
-400
-600
-800
Stress Component, σ_{xx} (MPa)
0
0.005
0.01
0.015
0.02
0.025
0.03
Time (sec)
$Z=h/2$
$Z=0$
$Z=-h/2$

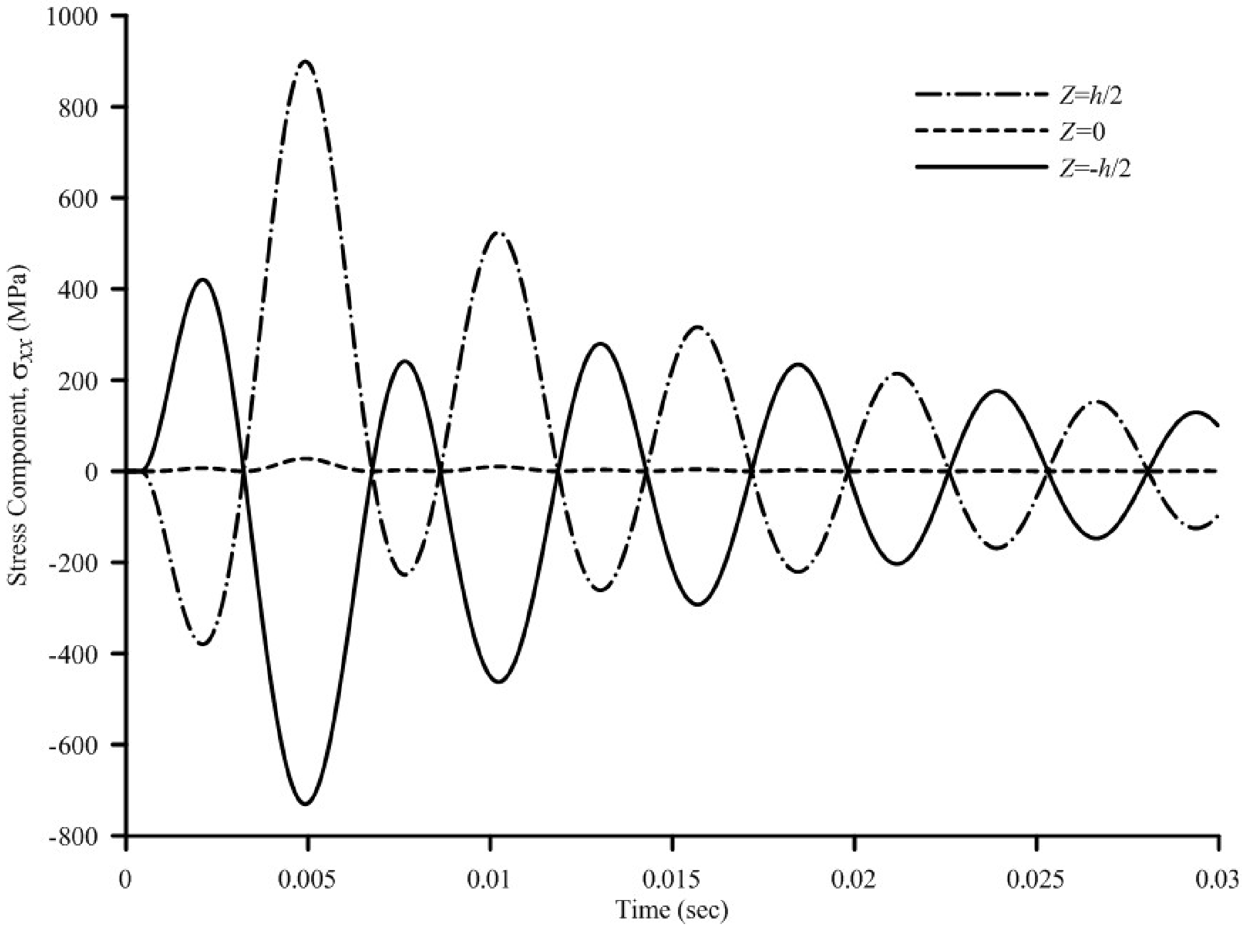
Z=h/2
Z=0
Z=-h/2
Stress Component, σxx (MPa)
1000
800
600
400
200
0
-200
-400
-600
-800
0
0.005
0.01
0.015
0.02
0.025
0.03
Time (sec)

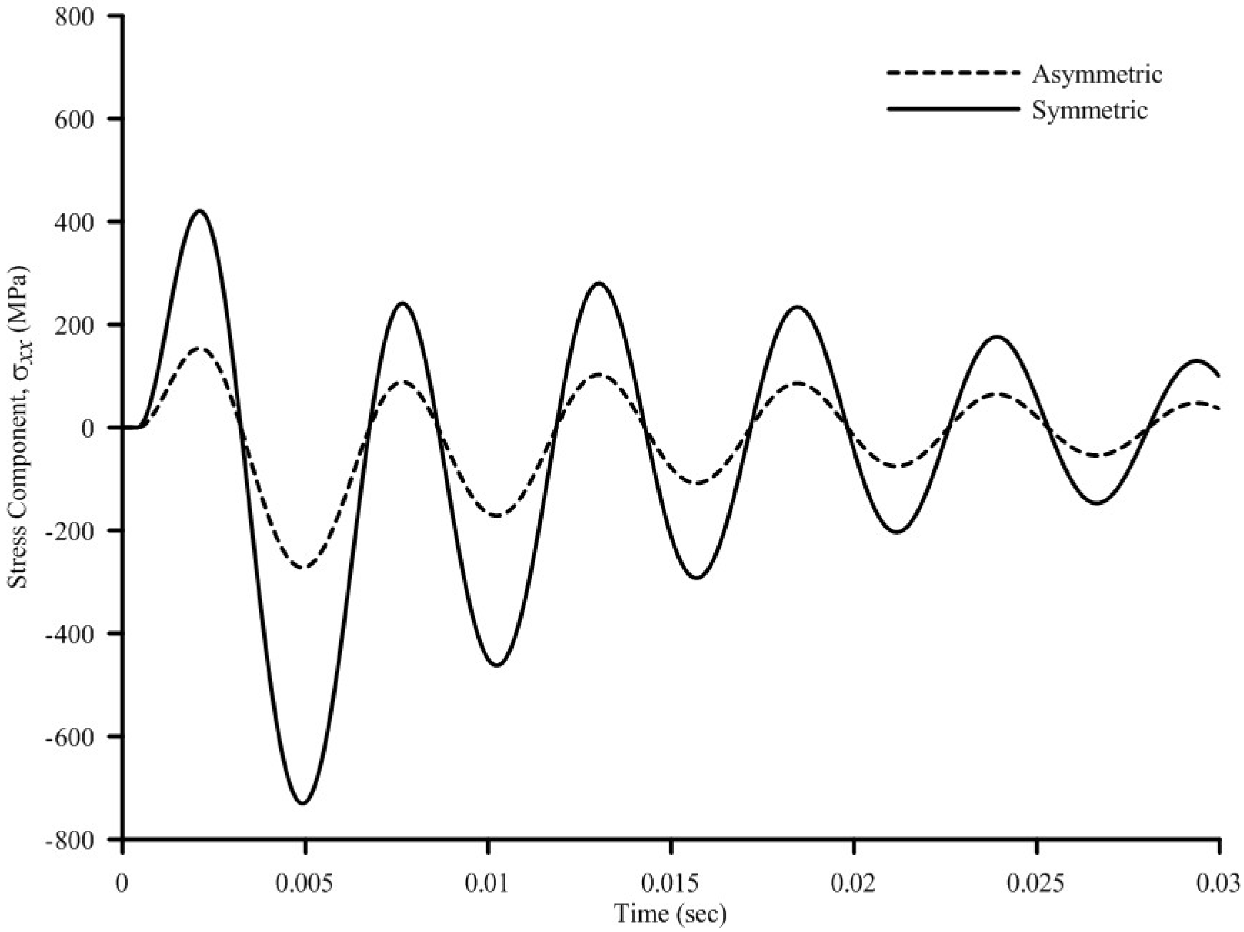
800
600
400
200
0
-200
-400
-600
-800
Stress Component, σ_{xx} (MPa)
0
0.005
0.01
0.015
0.02
0.025
0.03
Time (sec)
Asymmetric
Symmetric

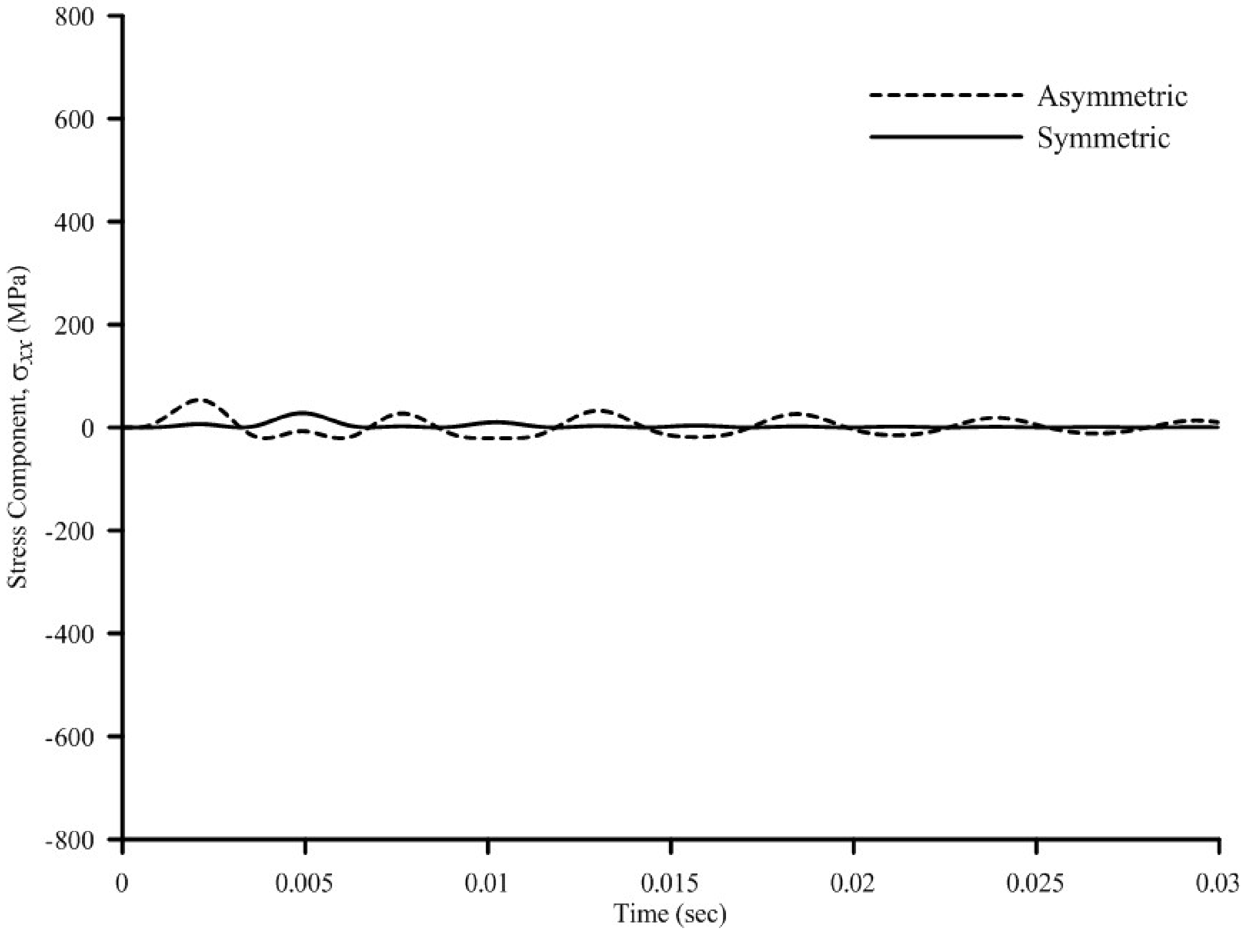
800
600
400
200
0
-200
-400
-600
-800
Stress Component, σ_{xx} (MPa)
Asymmetric
Symmetric
0
0.005
0.01
0.015
0.02
0.025
0.03
Time (sec)

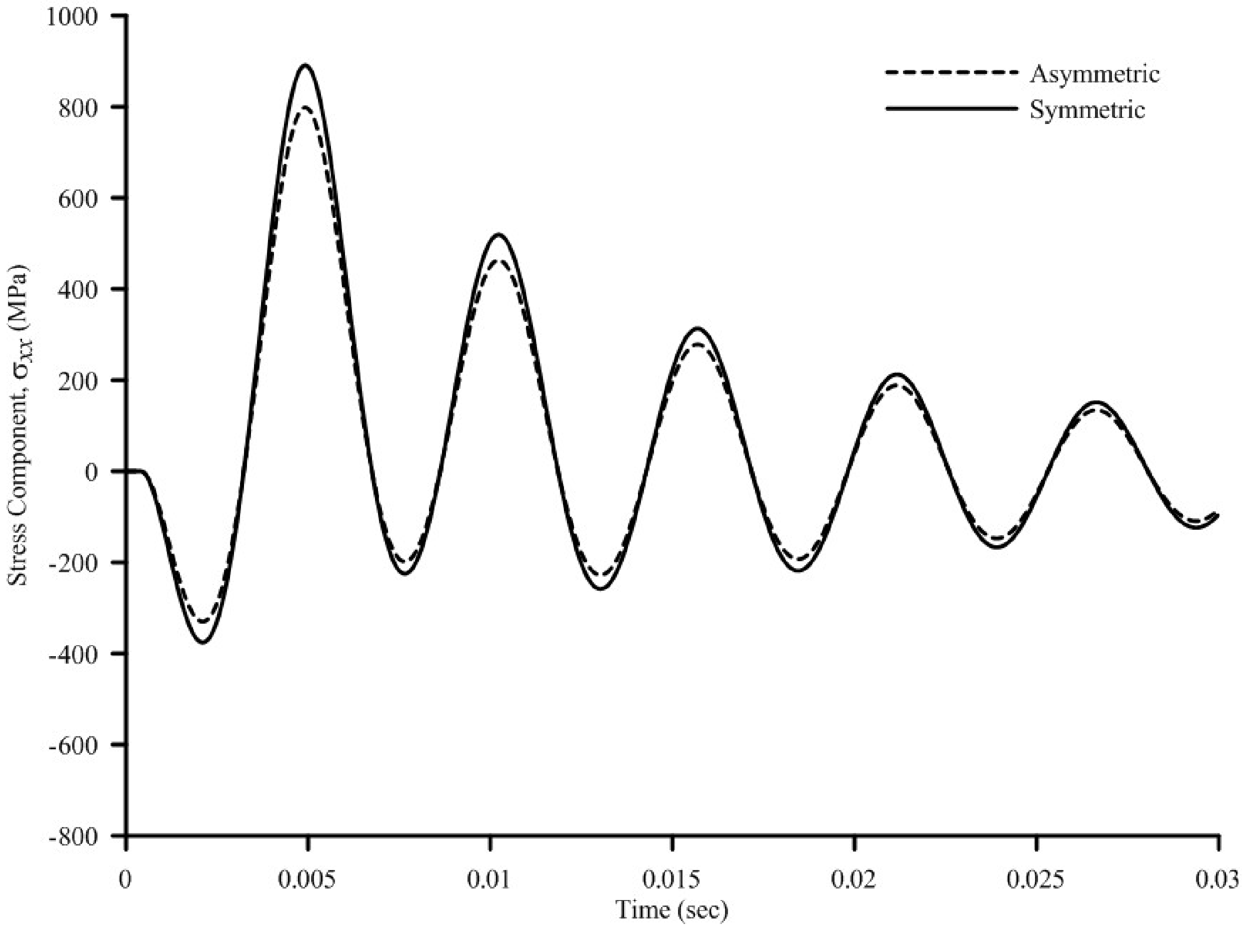
1000
800
600
400
200
0
-200
-400
-600
-800
Stress Component, σ_{xx} (MPa)
0
0.005
0.01
0.015
0.02
0.025
0.03
Time (sec)
Asymmetric
Symmetric